Progress in Applied Mathematics
Vol. 1, No. 1, 2011, pp. 71-89
www.cscanada.org

ISSN 1925-251X [Print]
ISSN 1925-2528 [Online]
www.cscanada.net

Linear Spatial Stability Analysis of Mixed Convection Boundary Layer over a Heated Plate

T. K. Sengupta[1,*]
S. Unnikrishnan[1]
S. Bhaumik[1]
P. Singh[1]
S. Usman[1]

Abstract: The spatial stability properties of a mixed convection boundary layer developed over a heated horizontal flat plate is investigated under the linear and quasi-parallel assumptions by solving the Orr-Sommerfeld equations. The main aim of this work is to find a critical buoyancy parameter above which a qualitative change in the stability characteristics of the mixed convection boundary layer due to the influence of heat transfer is displayed. The equilibrium flow used here is that given by the similarity solution of [1] which implies the wall temperature to vary as the inverse square root of the distance from the leading edge of the plate. The Orr-Sommerfeld equation has been solved by using the compound matrix method (CMM)– which locates all the modes in a chosen range of complex wave number, for spatial stability analysis. Cases with different buoyancy parameters have been investigated which were earlier reported incorrectly in [2]. Results indicate modifications of the hydrodynamic mode with certain buoyancy parameter for which continuous existence of instability as the flow develops downstream. The erroneous results in the above mentioned paper is associated with the wrong choice of compound variables used in CMM and the associated dispersion relation satisfied at the wall.

Key Words: Mixed Convection Flow; Orr-Sommerfeld Equation; Spatial Stability Analysis; Compound Matrix Method (CMM)

1. INTRODUCTION

Mixed convection flows are important as they are found in many practical situations in nature and man-made devices. Mixed convection flows differ from isothermal flows due to the induced buoyancy effects via heat transfer. It has been noted in [3] that in natural convection and in the mixed regime, instability occurs due to the growth of small disturbances. The unstable frequencies for natural convection fall within a small band whereas for forced convection it is much more wider. In some flows, as in flow past a vertical plate, induced body forces are either parallel or anti-parallel to the mean convection direction.

Flow and heat transfer properties are more complicated in the case of mixed convection flows over

[1]Department of Aerospace Engineering, I. I. T. Kanpur 208 016, India. E-mail address: tksen@iitk.ac.in.
[*]Corresponding author.
[†]Received 10 December 2010; accepted 11 January 2011.

horizontal and inclined plates since buoyancy forces induce longitudinal pressure gradient which alters the flow and heat transfer rates. This is evident from Equations (8) and (9) describing the mean flow. In addition to this, such imposed pressure gradients can also alter instability characteristics of flows. As instability in mixed convection flows starts off with the growth of small disturbances, linear stability theory is often used to study these flows. Traditionally, analysis has been performed using temporal theory, as in [4] for mixed convection flows along an isothermal vertical flat plate. The effect of buoyancy is studied by the temporal theory of a flow perturbed by small buoyancy-induced body force. The mean flow was obtained by local nonsimilarity method and they reported the buoyancy force to stabilize the assisting flow. One also notes the critique of various nonsimilar flow descriptions used in instability studies given in [3]. All nonsimilar methods using similarity are local in nature, with nonsimilar terms defined as new variables. The boundary layer equations are augmented by new equations obtained by differentiating the transformed boundary layer equation with respect to new variables. This process again lead to another equation which is again nonsimilar. If the previous process of creating augmented equations is repeated, the system never closes, unless at some level nonsimilar terms are omitted. According to the authors, *this measure makes the accuracy of local nonsimilarity method difficult to assess.* Having realized this , it was decided to obtain the stability of mixed convection flow given by a similarity solution given in [2]. This is revisited here, correcting the mistakes of the disturbance equation, while investigating larger ranges of buoyancy parameters.

Experimental studies relate to spatial growth of disturbances for flow system excited by fixed frequency sources. Hence, spatial theory is preferred to study instability of non-isothermal flows. Despite the distinction between spatial or temporal approach, the neutral curve remains the same. Results using linear spatial theory and parallel flow approximation have been reported for free-convection flow on inclined plates in [5]. The spatial stability of natural convection flow on inclined plates providing the eigenspectrum was reported in [6]. Here, the stability properties of a mixed convection boundary layer developed over a heated horizontal flat plate is investigated. Such a problem is of importance for engineering applications and geophysical fluid dynamics. We note that mixed convection over a cooled horizontal plate exhibit nonuniqueness. Numerical instability for the corresponding boundary layer equation is studied in [7].

When Boussinesq approximation is adopted in the full conservation equations, the buoyancy effect appears in terms of Gr/Re^2, where Gr is the Grashof number and Re is the Reynolds number defined in terms of appropriate length, velocity and temperature scales. However [8] have shown that the equivalent buoyancy parameter with the boundary layer assumption changes to $K = Gr/Re^{5/2}$. Experimental investigations in Refs. [9, 10] have demonstrated the onset of instability to always occur at the same value of K, underlying the importance of K as the relevant buoyancy parameter. The similarity profile derived in [1] is given in terms of K only.

The similarity solutions of [1] is used to study the stability characteristics of mixed convection boundary layer over a flat plate, as the benchmark results for a similarity profile obtained by an accurate method. It is known that heat addition to flow past a horizontal plate results in destabilizing the boundary layer, the present work aims to quantify it and check its dependence on buoyancy parameter.

As compared to the canonical problem of instability of flow past a plate for isothermal flow, the present study is complicated when heat transfer effects are introduced due to the increase in the order of the stability equation. It is known that viscous action can destabilize isothermal flows. Flow past a heated horizontal plate is further destabilized by the buoyancy forces and both these enhance instabilities.

Addition of heat transfer effects require solving energy equation, resulting in sixth order stability equation, instead of the fourth order equation solved for isothermal flows. In reporting results in [11], the authors have used Runge-Kutta integration scheme along with Kaplan filtering technique to avoid numerical difficulties. Ref. [6] has used both Chebyshev collocation and Runge-Kutta integration schemes to solve the ninth order stability equation. In collocation method 70 modes were taken and Runge-Kutta method required Gram-Schmidt orthonormalization procedure to maintain linear independence of the components of fundamental solutions. The major difficulty in studying instability is due to fundamental solutions dis-

playing variation of physical quantities at totally dissimilar rates, which is the stiffness problem. This problem is tackled by special techniques for solving the stability equations as described in [12] and [13]. Here we focus on shooting method using Compound Matrix Method (CMM). According to [14], spurious eigenvalues are created due to fracturing of the continuous spectrum for problems in infinite domain. In [15], a QR algorithm based Chebyshev polynomials have been used for the spatio-temporal study of mixed convection boundary layers developing over a vertical plate. Ref. [14] have noted that orthogonalization/orthonormalization procedure causes numerical solution to be nonanalytic and on infinite domains there is the added problem that asymptotically correct boundary conditions may not preserve analyticity. CMM does not suffer from any of these problems. Basic ideas behind CMM are given in [16] and [17]. CMM has been re-developed using exterior algebra in a co-ordinate free context in [16]. CMM has been used in [18] for receptivity analysis and reporting the eigenspectrum of Blasius boundary layer. Some problems of CMM has been identified and solved in [19] to obtain eigenfunctions correctly for high wave numbers. In [14], the stability problem of Ekman boundary layer interacting with a compliant surface has been studied by solving a sixth-order system by CMM. In [17], CMM has been developed for general forth-and sixth-order systems. CMM avoids creating spurious eigenvalues while retaining the analyticity of dispersion relation and mainly makes a method available that exploits the analytic structure of the solution.

The governing equations are given in the next section. The mean flow, whose stability will be studied, is given is section 3. The stability equations and related numerical methods for CMM are given in section 4. The results and discussion follow in section 5. The paper closes with summary and conclusions in section 6.

2. GOVERNING EQUATIONS AND FORMULATION

A laminar two-dimensional flow of a fluid past a semi-infinite horizontal plate is considered. The free stream velocity and temperature are denoted by U_∞ and T_∞ respectively. We concentrate attention on the upper surface of the plate and that has a surface temperature distribution T_w, which is greater than T_∞ and assume the leading edge to be a stagnation point. The governing equations in dimensional form (indicated by quantities in asterik),–with Boussinesq approximation to represent the buoyancy effect–for velocity and temperature fields are given as,

$$\nabla^*.\vec{V^*} = 0, \tag{1}$$

$$\frac{D\vec{V^*}}{Dt^*} = g_j\beta(T^* - T_\infty) - \frac{1}{\rho}\nabla p^* + \nu\nabla^2\vec{V^*}, \tag{2}$$

$$\frac{DT^*}{Dt^*} = \alpha\nabla^{*2}T^* + \frac{\nu}{C_p}\phi_v + \frac{q}{\rho C_v}, \tag{3}$$

where $\frac{D}{Dt^*}$ represents the substantial derivative and ϕ_v and q are the viscous dissipation and heat generation terms in the energy equation. Also, $g_j = [0,\ g,\ 0]^T$ is the gravity vector; α and ν are the thermal diffusivity and kinematic viscosity, respectively; β represents the volumetric thermal expansion coefficient. In the following analysis, the viscous dissipation (ϕ_v) and heat generation term (q) are neglected.

Above equations are non-dimensionalised by introducing a length scale (L), temperature scale ($\Delta T = T_w - T_\infty$) and pressure scale ($\rho U_\infty^2$) which yield,

$$\nabla.\vec{V} = 0, \tag{4}$$

$$\frac{D\vec{V}}{Dt} = \frac{Gr}{Re^2}T - \nabla p + \frac{1}{Re}\nabla^2\vec{V}, \tag{5}$$

$$\frac{DT}{Dt} = \frac{1}{RePr}\nabla^2 T^*, \tag{6}$$

where $T = (T^* - T_\infty)/\Delta T$; $Gr = \frac{g\beta\Delta T L^3}{\nu^2}$; $Re = \frac{U_\infty L}{\nu}$ and $Pr = \frac{\nu}{\alpha}$. The term $\frac{Gr}{Re^2}$ in the momentum equation is known as the Richardson number or Archimedes number. The Grashof number (Gr) weighs the relative importance of buoyancy and viscous terms. Richardson number/Archimedes number is of order one in the mixed convection regime.

3. MEAN FLOW EQUATIONS

The mean flow equations are obtained by applying the boundary later approximation to the above governing equations. For a two-dimensional (2D) incompressible flow, the non dimensional equations in a Cartesian co-ordinate system, (fixed at the leading edge of the plate), are given in [1] as

$$\frac{\partial U}{\partial X} + \frac{\partial V}{\partial Y} = 0, \tag{7}$$

$$U\frac{\partial U}{\partial X} + V\frac{\partial U}{\partial Y} = -\frac{\partial P}{\partial X} + \frac{\partial^2 P}{\partial Y^2}, \tag{8}$$

$$0 = K\theta - \frac{\partial P}{\partial Y}, \tag{9}$$

$$U\frac{\partial \theta}{\partial X} + V\frac{\partial \theta}{\partial Y} = \frac{1}{Pr}\frac{\partial^2 \theta}{\partial Y^2}, \tag{10}$$

where $X = x/L$; $Y = y\sqrt{Re}/L$; $U = u/U_\infty$; $V = \sqrt{Re}v/U_\infty$; $\theta = \frac{T-T_\infty}{T_w-T_\infty}$; $P = p/(\rho_\infty U_\infty^2)$; and $K = Gr/Re^{5/2}$. These equations are solved subject to the following boundary conditions. At the wall ($Y = 0$ and $X > 0$): $U = V = 0$ and at the free stream($Y \to \infty$): $U = 1$ and $\theta = P = 0$.

In the above set of equations, (7) is automatically satisfied if we introduce a stream function (ψ). As P indicates an excess pressure over the free-stream value, (9) can be integrated to give, $P = -\int_Y^\infty K\theta dY$. When these are introduced in the x-momentum and the energy equations, one gets

$$\psi_Y\psi_{XY} - \psi_X\psi_{YY} - K\int_Y^\infty \theta_X dY = \psi_{YYY}, \tag{11}$$

$$\psi_Y\theta_X - \psi_X\theta_Y = \frac{1}{Pr}\theta_{YY}. \tag{12}$$

The buoyancy force creates a streamwise pressure gradient given by $K\int_Y^\infty \theta_X dY$ in (11). This makes the mean flow nonsimilar. But, in [1], it has been shown that the above formulation admits a similarity solution, if $\theta_w \propto X^{-1/2}$ for which the following similarity transformations are introduced for the independent variable: $\eta = YX^{-1/2}$ and for the dependent variables via: $\psi = X^{1/2}g(\eta)$ and $\theta = \theta_w\Theta$. These transformations yield the following system of equations:

$$2g''' + gg'' + K\eta\Theta = 0, \tag{13}$$

$$\frac{2}{Pr}\Theta'' + g\Theta' + g'\Theta = 0. \tag{14}$$

In these equations, a prime indicates a derivative with respect to η, the independent variable. These equations have to be solved subject to the following boundary conditions. At $\eta = 0$: $g = g' = 0$ and $\Theta = 1$ and as $\eta \to \infty$: $g' = 1$ and $\Theta = 0$. The energy equation can be integrated analytically once to obtain

$$\frac{2}{Pr}\Theta' + g\Theta = 0. \tag{15}$$

This equation can be further integrated analytically to yield Θ, once g is obtained as a solution of Equation (3.7). Note that the solutions depend on Reynolds number, that is implicitly include in the Y or η co-ordinate. The numerical results of these are presented in [1]. From (15), it can be seen that the slope of Θ at wall is zero irrespective of K, which implies that this solution is for adiabatic condition over the plate.

4. STABILITY EQUATIONS AND NUMERICAL METHOD

The stability equations for 2D plane flows is derived starting from the nondimensional equations (4)-(6) given by

$$\frac{\partial u}{\partial x} + \frac{\partial v}{\partial y} = 0, \tag{16}$$

$$\frac{\partial u}{\partial t} + u\frac{\partial u}{\partial x} + v\frac{\partial u}{\partial y} = -\frac{\partial p}{\partial x} + \frac{1}{Re}\Big[\frac{\partial^2 u}{\partial x^2} + \frac{\partial^2 u}{\partial y^2}\Big], \tag{17}$$

$$\frac{\partial v}{\partial t} + u\frac{\partial v}{\partial x} + v\frac{\partial v}{\partial y} = \frac{Gr}{Re^2}T - \frac{\partial p}{\partial y} + \frac{1}{Re}\Big[\frac{\partial^2 v}{\partial x^2} + \frac{\partial^2 v}{\partial y^2}\Big], \tag{18}$$

$$\frac{\partial T}{\partial t} + u\frac{\partial T}{\partial x} + v\frac{\partial T}{\partial y} = \frac{1}{RePr}\Big[\frac{\partial^2 u}{\partial x^2} + \frac{\partial^2 u}{\partial y^2}\Big]. \tag{19}$$

For the stability analysis, the physical variables are split into a mean part, derived in section 3, and a fluctuating component indicated by a caret in the following:

$$u(x, y, t) = \bar{U}(x, y) + \epsilon\hat{u}(x, y, t), \tag{20}$$

$$v(x, y, t) = \bar{V}(x, y) + \epsilon\hat{v}(x, y, t), \tag{21}$$

$$p(x, y, t) = \bar{P}(x, y) + \epsilon\hat{p}(x, y, t), \tag{22}$$

$$T(x, y, t) = \bar{T}(x, y) + \epsilon\hat{t}(x, y, t). \tag{23}$$

The quantities with the over-bar are related to the mean flow solutions of the previous section, via appropriate transformations. The stability equations are obtained by making the additional parallel flow assumption, $\bar{U} = \bar{U}(y)$, $\bar{V} = 0$ and $\bar{T} = \bar{T}(y)$ so that a normal mode spatial instability analysis is possible by looking for a solution of the linearized equations of the following form:

$$[\hat{u},\ \hat{v},\ \hat{p}, \hat{T}] = [f(y),\ \phi(y),\ \pi(y),\ h(y)]\ e^{i(kx-\omega t)}. \tag{24}$$

After substituting (24) into (16) to (19), one gets the system of equations governing the disturbance amplitude function as,

$$i(k\bar{U} - \omega)(k^2\phi - \phi'') + ik\bar{U}''\phi = \frac{Gr}{Re^2}k^2 h - \frac{1}{Re}(\phi^{iv} - 2k^2\phi'' + k^4\phi), \tag{25}$$

$$i(k\bar{U} - \omega)h + \bar{T}'\phi = \frac{1}{RePr}(h'' - k^2 h). \tag{26}$$

These are the well known Orr-Sommerfeld equations for mixed convection flows which show the disturbance normal velocity and the temperature fields to be coupled, constituting a sixth order differential system. Equations (25) and (26) are solved subject to the six boundary conditions:

$$at\ y = 0 : \phi, \phi' = 0, h = 0, \tag{27}$$

$$as\ y \to \infty : \phi, \phi', h \to 0. \tag{28}$$

The homogeneous boundary conditions for h at the wall corresponds to the eigenvalue analysis, in contrast to receptivity analysis where $h = h(x, t)$ is prescribed at the wall to represent specific thermal input. It was shown in [18] that receptivity and stability analysis are related through the disturbance amplitude expression. The general solution to the coupled system of ODEs can be represented as

$$\phi = a_1\phi_1 + a_2\phi_2 + a_3\phi_3 + a_4\phi_4 + a_5\phi_5 + a_6\phi_6, \tag{29}$$

$$h = a_1h_1 + a_2h_2 + a_3h_3 + a_4h_4 + a_5h_5 + a_6h_6. \tag{30}$$

Indicated boundary conditions imply the disturbances to decay in the far stream, ($y \to \infty$). Equations (25) and (26) with boundary conditions (27) and (28) indicate that the temperature field given by (26) decouples from the velocity field in the free stream where $\bar{T}' \approx 0$. Thus the free stream energy equation reduces to,

$$h'' - [iRePr(k-\omega) + k^2]h = 0. \tag{31}$$

The characteristic modes at free stream are given by

$$h_\infty = a_5e^{-Sy} + a_6e^{Sy}, \tag{32}$$

where $S = \sqrt{k^2 + iRePr(k-\omega)}$. To satisfy the free stream boundary condition, we have $a_6 = 0$ for real(S) > 0. It can be seen that as $y \to \infty$, $h_{1\infty} = h_{3\infty} = 0$. At the free stream, momentum equation gives

$$\phi^{iv} - [2k^2 + iRe(k-\omega)]\phi'' + [k^4 + iRe(k-\omega)k^2]\phi = Re\sqrt{Re}Kk^2h. \tag{33}$$

Here, $\bar{U} = 1$ and all mean flow derivatives are 0. This reveals that, at the free stream, momentum equation is not decoupled from the thermal field. This equation for disturbance amplitude of normal component of velocity represents a forced dynamics with the thermal field acting as the forcing. The homogeneous part of this equation has the solution,

$$\phi_H = a_1e^{-ky} + a_2e^{ky} + a_3e^{-Qy} + a_3e^{Qy}, \tag{34}$$

where $Q = \sqrt{k^2 + iRe(k-\omega)}$. To satisfy the free stream conditions, we must have $a_2 = a_4 = 0$ for real(K, Q)> 0. Using the expression for h_∞ from (32) and the relation $a_6 = 0$, the particular integral, for the above ODE can be found out as follows. The momentum equation at free stream:

$$\phi^{iv} - (k^2 + Q^2)\phi'' + k^2Q^2\phi = Re\sqrt{Re}Kk^2a_5e^{-Sy}. \tag{35}$$

Particular integral:

$$\phi_{PI} = \frac{a_5Re\sqrt{Re}Kk^2}{S^4 - (k^2+Q^2)S^2 + k^2Q^2}e^{-Sy}. \tag{36}$$

Hence we can write the solution of the coupled momentum and energy equations at the free stream as,

$$\phi = a_1e^{-ky} + a_3e^{-Qy} + a_5\gamma e^{-Sy}, \tag{37a}$$

$$h = a_5e^{-Sy}, \tag{37b}$$

where $h_1 = h_3 = 0$, $Q = \sqrt{k^2 + iRe(k-\omega)}$, $S = \sqrt{k^2 + iRePr(k-\omega)}$ and $\gamma = \frac{Re\sqrt{Re}Kk^2}{S^4-(k^2+Q^2)S^2+k^2Q^2}$ with the real part of k,Q and S positive. The governing stability equations can be represented as a system of six first order equations by introducing the the vector:

$$\mathbf{u}(y,.) = [u_1(y,.), u_2(y,.), u_3(y,.), u_4(y,.), u_5(y,.), u_6(y,.)]^T, \tag{38}$$

where $u_1 = \phi, u_2 = \phi', u_3 = \phi'', u_4 = \phi''', u_5 = h, u_6 = h'$. Note that this definition is different from that was written in [2]. Despite this difference, the governing equations in terms of the twenty compound variables are identical, as given by Equation(A.3) in [2]. However, the dispersion relation was taken wrongly in [2]. The governing system of equations given by (25) and (26) can be written as

$$u_j' = [A]u_j, \tag{39}$$

where u is defined by $u \in C^6$ and the matrix $[A]$ is written as

$$\begin{bmatrix} 0 & 1 & 0 & 0 & 0 & 0 \\ 0 & 0 & 1 & 0 & 0 & 0 \\ 0 & 0 & 0 & 1 & 0 & 0 \\ -a & 0 & b & 0 & c & 0 \\ 0 & 0 & 0 & 0 & 0 & 1 \\ e & 0 & 0 & 0 & d & 0 \end{bmatrix},$$

with $a = k^4 + iRek\bar{U}'' + iRek^2(k\bar{U} - \omega)$; $b = 2k^2 + iRe(k\bar{U} - \omega)$; $c = k^2\frac{Gr}{Re}$; $d = k^2 + iRePr(k\bar{U} - \omega)$; and $e = RePr\bar{T}'$. Equation (39) has to be integrated on C^6 defined on $y \in [0, \infty]$ with three boundary conditions at wall defined by (27) and three asymptotic conditions as $y \to \infty$ defined by (28). The integration of (39) subject to boundary conditions (27) and (28) is not straightforward–due to the stiffness problem of the governing ODEs. To circumvent this stiffness problem and to integrate the governing equations we use the CMM–as described in detail in the appendix.

4.1 Dispersion Relation

To solve the stability problem the CMM equations given by (A.3) in [2] are to be solved starting from $y = y_\infty$ using the initial conditions given in the Appendix. The dispersion relation is obtained by satisfying the wall boundary conditions given by (27) in terms of disturbance velocity components and temperature field. In terms of fundamental solution components, these conditions at the wall can be written as,

$$a_1\phi_1 + a_3\phi_3 + a_5\phi_5 = 0, \tag{40}$$

$$a_1\phi_1' + a_3\phi_3' + a_5\phi_5' = 0, \tag{41}$$

$$a_1h_1 + a_3h_3 + a_5h_5 = 0. \tag{42}$$

Thus, the dispersion relation can be obtained from the characteristic determinant of the linear system formed by (40), (41) and (42). After simplification and using the definitions of second compounds, the dispersion relation is obtained as

$$D_r + iD_i = y_3 = 0 \;\; at \;\; y = 0. \tag{43}$$

The dispersion relation has an interesting physical and mathematical interpretation that can be understood in the context of spatio-temporal receptivity analysis, as given in [18] for the excitation problem of a parallel shear layer. For the isothermal flow analyzed therein, if the fundamental decaying solutions are identified as ϕ_1 and ϕ_3, then the disturbance stream function is shown as

$$\psi(x, y, t) = \frac{1}{(2\pi)^2}\int\int \frac{\phi_1'\phi_{30} - \phi_3\phi_{10}'}{\phi_{30}'\phi_{10} - \phi_{30}\phi_{10}'} BC_w e^{i(kx-\omega t)} dkd\omega, \tag{44}$$

where the subscript "0" refers to the quantities evaluated at the wall and BC_w is the excitation provided at the wall. For isothermal flow, the denominator of the integrand on the right-hand side of the Fourier-Laplace integral is the dispersion relation of the corresponding eigenvalue problem. Thus, it is very easy to see that the dispersion relation provides the poles for the receptivity problem, that will yield the asymptotic solution obtained using residue theorem. In the context of the present problem, if one is interested in a receptivity analysis with respect to wall excitation, then in Equation (27) one of the wall conditions would be inhomogeneous and identified with BC_w in (44). Also in (44) the denominator will have to be replaced with the dispersion relation given by Equation (43) and the numerator would change in terms of the fundamental solutions, ϕ_1, ϕ_3 and ϕ_5. The present study is focused upon the the corresponding eigenvalue problem and the discussion is to show the importance of the dispersion relation. Readers can look at [18] for further details on spatio-temporal receptivity analysis.

This completes the definition of stability problem of mixed convection flow past a horizontal plate. For a given K, Re and Pr, one would be required to solve Equation (A.3) in [2], starting with initial conditions given in the Appendix and satisfy (43) for particular combinations of eigenvalues obtained as complex k and ω. The procedures adopted in [18] are used to obtain the eigenspectrum for the mixed convection case, when the problem is analyzed by spatial theory. In this process, it is possible to scan for all eigenvalues in the complex k-plane, without any problem of spurious eigenvalues.

4.2 Eigenfunction for the Mixed Convection Problem

Once we obtain the eigenvalues using the CMM we can solve for the eigenfunction. The eigenfunctions could be written in terms of the decaying fundamental modes as

$$\phi = a_1\phi_1 + a_3\phi_3 + a_5\phi_5. \tag{45}$$

For the sixth order system, one can form the auxiliary system of equations by eliminating a_1, a_3 and a_5 from the definition of the second compounds as provided in the Appendix and

$$\phi' = a_1\phi_1' + a_3\phi_3' + a_5\phi_5', \tag{46}$$

$$\phi'' = a_1\phi_1'' + a_3\phi_3'' + a_5\phi_5'', \tag{47}$$

$$\phi''' = a_1\phi_1''' + a_3\phi_3''' + a_5\phi_5'''. \tag{48}$$

Using (45)-(47) and using the definition of the second compounds, one obtains the following axillary equation:

$$y_1\phi''' - y_2\phi'' + y_5\phi' - y_{11}\phi = 0. \tag{49}$$

If instead one uses (45), (46) and 4.28, the following equation is obtained:

$$y_1\phi^{iv} - y_3\phi'' + y_6\phi' - y_{12}\phi = 0. \tag{50}$$

There are many other possible auxiliary equations that can be used in principle to obtain the eigenfunctions. In the context of fourth-order systems, multiplicity of such equations was considered a source of confusion [12]–that was resolved later in [19] by looking at the eigenfunction equations for their correct asymptotic behaviour when $y \to Y_\infty$. As the problem allows only three decaying modes for the present case, it is necessary to ensure that the chosen eigenfunction equation also displays the same asymptotic decay. Equation (49) displays the correct decay rates of $-k$, $-Q$ and $-S$, while (50) has the asymptotic variation given by the characteristic exponents as $-k$, $-Q$, $-S$ and $(k + S + Q)$. Thus Equation (50) has a spurious, violently growing mode and cannot be used. As Equation (49) shows correct solution behaviour, we will not look for any further auxiliary equations.

5. RESULTS AND DISCUSSION

First, the mean flow is obtained by solving (13) and (15) by standard four-stage Runge-Kutta method. These equations are solved by taking the maximum similarity co-ordinate, $\eta_{max} = 12$ which is equally divided into 4000 sub-intervals. For different Re and K, mean flow has been obtained here. K is varied here since , for mixed convection flows, K is more important than Gr. As we have investigated the mixed convection problem in air, we have fixed the value of $Pr = 0.7$ for all cases. Obtained mean-flow results for nondimensional velocity, its second derivative, temperature and its first derivative have been shown for two values of K in Figures 1 and 2.

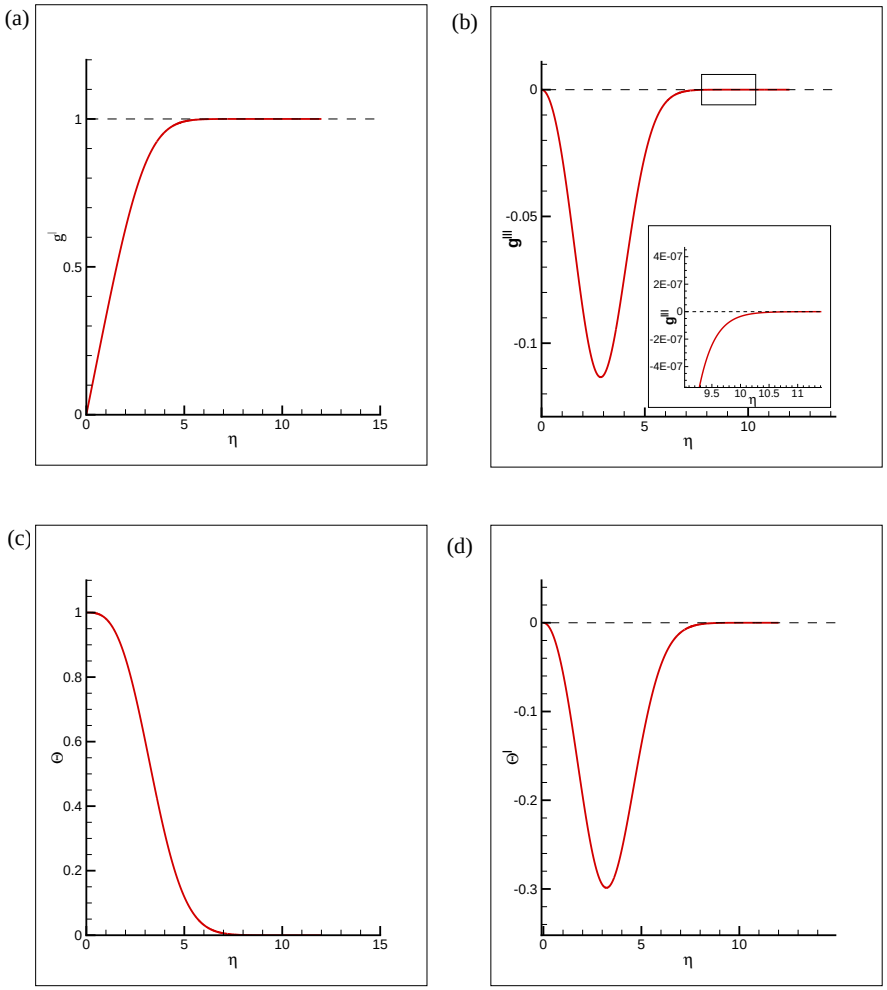

Figure 1: The variation of mean flow quantities for $K = 1 \times 10^{-6}$

5.1 Eigenspectrum for Mixed Convection Problem

Mean flow is obtained using the similarity co-ordinate η, while the stability equations are solved using the independent variable, $y = \frac{y^*}{\delta^*}$, where y^* is the dimensional height over the plate and δ^* is the displacement thickness of the boundary layer. In terms of η, the displacement thickness is given by

$$\delta^* = \sqrt{\frac{\nu x}{U_\infty}} \int_0^\infty [1 - g'(\eta)] d\eta = \sqrt{\frac{\nu x}{U_\infty}} C_m. \tag{51}$$

Thus the two ordinates are related by $y = \eta / C_m$ and C_m depends upon the choice of K. For $K = 0$(the Blasius profile) this is obtained as 1.72089, while for $K = 0.1$ this reduces to 1.13831. As all our investigations are related to the events on top of the plate, K is non negative and these two values provide

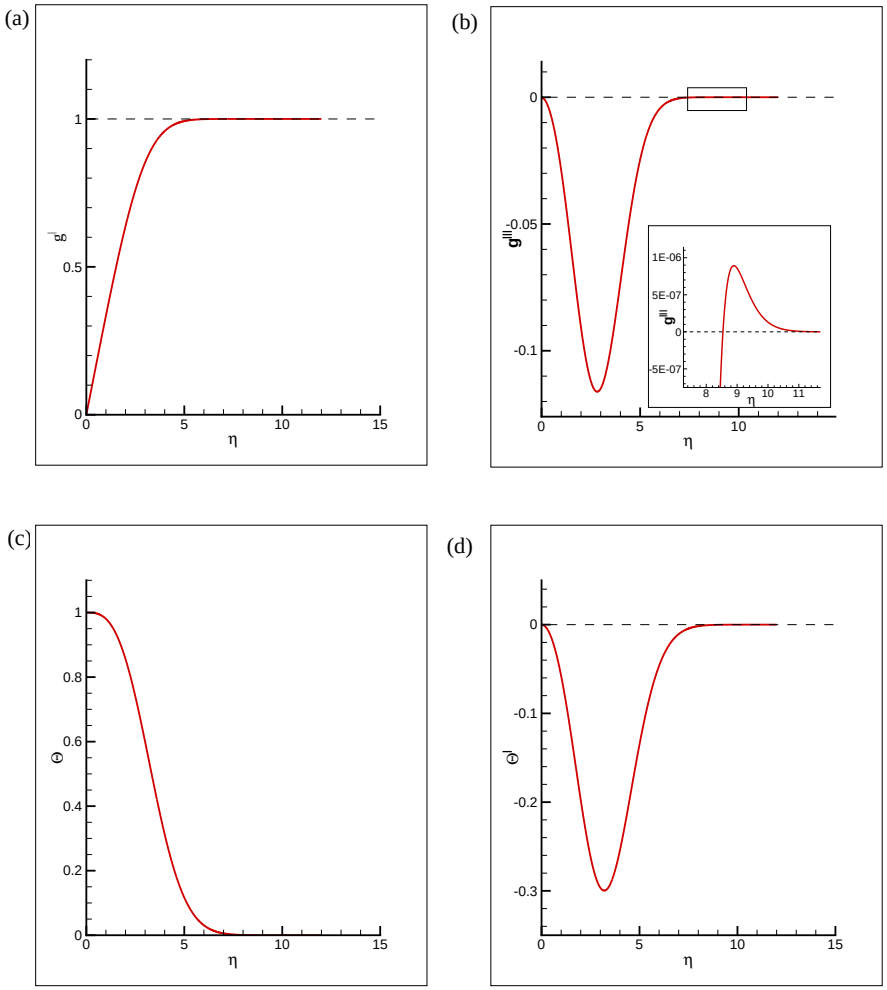

Figure 2: The variation of mean flow quantities for $K = 3 \times 10^{-3}$

the outer limits. In the present study, linear analysis has been done over various values of K starting from 1×10^{-6} to 2×10^{-2}.

To obtain the eigenspectrum for the spatial stability analysis, the induced system of equations are solved from freestream to wall, for fixed Re and K, and $\omega = \omega_0$ and any guess value of complex k. Due to the use of Runge-Kutta method, the stability equations are solved with 2000 sub-intervals between Y_∞ and the wall. For incorrect guess of k, $(D_r + iD_i)$ will not be equal to zero. To obtain approximate values of k quickly, we scan the complex-k plane for points where D_r and D_i are simultaneously zero. This global method for finding sets of eigenvalues not requiring iteration, is followed by a Newton-Raphson search procedure where the guessed values are polished off to the desired degree of accuracy and reported here. The same technique is followed in [18] for obtaining the eigenspectrum of Blasius profile. This two step procedure is fast and pose no difficulties with CMM and is devoid of problems of finding any

spurious eigenvalues–as with matrix/spectral methods. The same procedure can also be used along with orthogonalization/orthonormalization method that follows a similar process of integrating from freestream to the wall. However such integration procedures are time consuming because of orthonormalization and hence difficult.

Table 1: Eigenspectrum and associated wave properties for $Re = 1000$; $K = 0$; $\omega_0 = 0.1$

Mode	k_{real}	k_{imag}	Phase Speed	Group Velocity
1	0.2798275	-0.0072872	0.3573630	0.4201681
2	0.1380388	0.1099129	0.7244340	0.4175365
3	0.1220118	0.1739385	0.8195929	0.8532714
4	0.2885657	0.2877180	0.3465415	0.2322288
5	0.1251551	0.1213782	0.7990086	0.3021148

Table 2: Eigenspectrum and associated wave properties for $Re = 1000$; $K = 1 \times 10^{-5}$; $\omega_0 = 0.1$

Mode	k_{real}	k_{imag}	Phase Speed	Group Velocity
1	0.2797056	-0.0073132	0.3575188	0.4201681
2	0.1379987	0.1098773	0.7246445	0.4173623
3	0.1220080	0.1739829	0.7989607	0.8525149
4	0.2885573	0.2877290	0.3465516	0.2320724
5	0.1251626	0.1213676	0.7989607	0.5327651

Table 3: Eigenspectrum and associated wave properties for $Re = 1000$; $K = 1 \times 10^{-5}$; $\omega_0 = 0.65$

Mode	k_{real}	k_{imag}	Phase Speed	Group Velocity
1	2.8626073	1.9128085	0.2270657	0.1698370
2	2.0203028	2.0166021	0.3217340	0.2221383
3	1.9268345	2.8522266	0.3373409	0.1787949
4	1.3078068	1.2989593	0.4970153	1.6778524
5	1.2829128	0.9604713	0.5066595	0.1887149
6	0.9475503	0.2504354	0.6859794	1.1737089

In [2], a case with $Re = 1000$ and $\omega_0 = 0.1$ is discussed. The same case is reproduced here using the new formulation. In addition to the three modes, two stable and one unstable, reported in [18] obtained by solving a fourth order ODE, here we get two stable modes. The phase speed is evaluated as $c = \omega_0/k_{real}$ and the group velocity as $V_g = \left.\frac{d\omega_0}{dk}\right|_{real}$. These modes are thus identified as hydrodynamic mode. The additional fourth and fifth eigenmode in Table 1 can be attributed to the disturbance energy Equation (26). For $K \neq 0$ such distinctions are undesirable as all the modes are coupled together. The sign of the group velocity is used to find out the propagation direction of corresponding disturbances, following [20] and [21]. Accordingly, all the modes shown in Table 1 are downstream propagating. This match between the present sixth-order system and the Blasius profile results in [18] provides one of the validation for the developed methodology for solving the stability equations for the sixth-order system. Next, the eigenspectrum is obtained for the mixed convection case with $K = 1 \times 10^{-5}$ and $Re = 1000$. For a choice of $\omega_0 = 0.1$, located eigenvalues and their wave properties are given in Table 2. Here also it can be seen that we get five

modes with properties similar to that of case with $K = 0$. The first mode represents an unstable mode and the rest four are stable. In [2], only three modes were obtained for this case. It was seen that in the present calculations, the phase speed is comparatively greater and growth rate lesser than those reported in [2]. In the present calculations, the group velocities were almost similar to earlier case. In Table 3, eigenspectrum for the case $K = 1 \times 10^{-5}$, $Re = 1000$ and $\omega_0 = 0.65$ is shown. The results indicate the presence of six eigenmodes which are all stable. The high values of k_{imag} for first five modes show that they are highly damped. The fourth and sixth modes have high values of group velocity which implies that the disturbance energy associated with these modes are convected away at a higher speed than the freestream speed. Due to the high damping rates and group velocity, these modes do not affect the dynamics.

5.2 Neutral Curves for Mixed Convection Problem

One primary aim of these studies is to find out critical value of parameters that indicate the onset of instability. Here the onset parameters are the critical Reynolds number (Re_{cr}) and the critical circular frequency (ω_{cr}). This work also probes the existence of a critical buoyancy parameter (K_{cr}) at which the instability properties change qualitatively as well as quantitatively as reported in [2]. We have seen that for $K = 0$, the coupled momentum and energy equations exhibit two additional stable modes in addition to the modes obtained for Blasius solution.The neutral curve for the mixed convection problem is obtained for various buoyancy parameters.

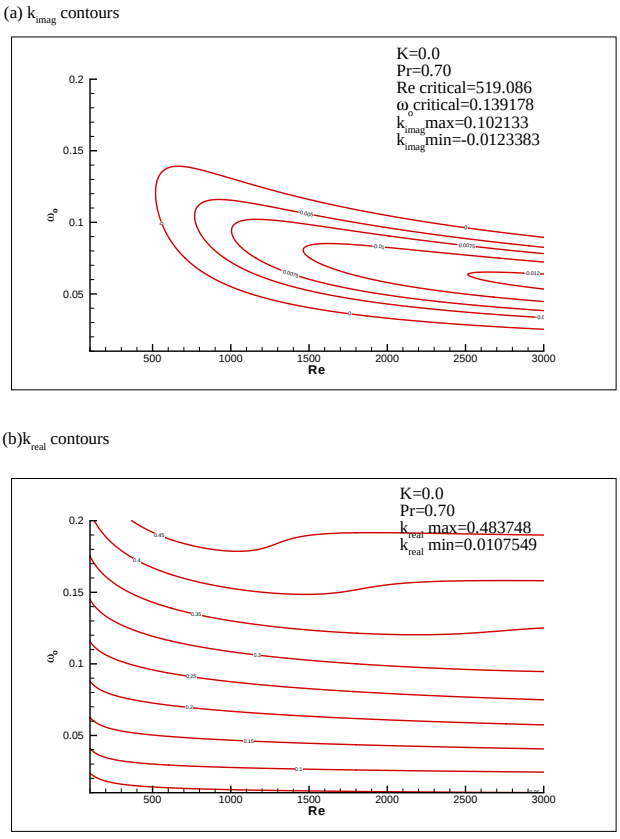

Figure 3: Wave number (k) contours for $K = 0$. Figure 3(a) shows the imaginary part of k and Figure 3(b) shows the real part of k

(a) k_{imag} contours

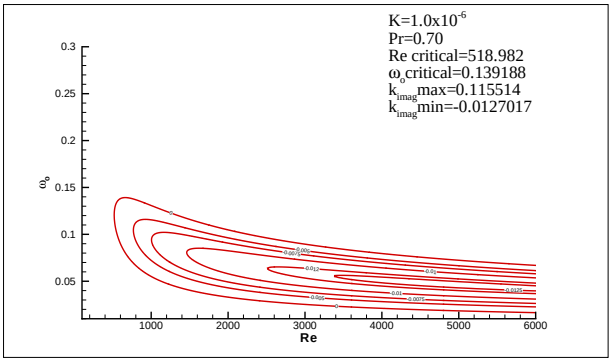

(b)k_{real} contours

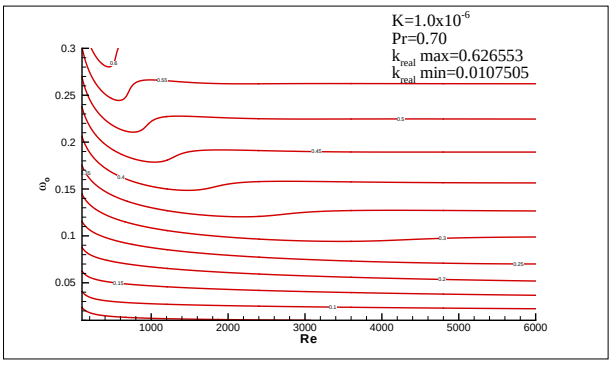

Figure 4: Wave number (k) contours for $K = 1 \times 10^{-6}$. Figure 4(a) shows the imaginary part of k and Figure 4(b) shows the real part of k

Figure 3(a) shows the neutral curve for $K = 0$. The critical Reynolds number (Re_{cr}) is 519.086 and the critical circular frequency (ω_{cr}) is 0.139178, which are identical to that obtained independently for Blasius profile. The critical parameters for various cases tested are given in Table 4. In Figure 4(a) the neutral curve is shown for the case $K = 1 \times 10^{-6}$. Here, one notices a lowering of Re_{cr}= 513.6 and ω_{cr}=0.139188. For the cases $K = 3 \times 10^{-6}$ and $K = 4 \times 10^{-6}$, Re_{cr} decreases and ω_{cr} increases marginally. The single lobed nature of the neutral curve is as in the Blasius profile case.

For the case $K = 5 \times 10^{-6}$, in [2] it was reported that in addition to the hydrodynamic mode, the neutral curve showed a second lobe. This second lobe existed at higher ω range and showed onset of instability at very low Reynolds number. Thus there were two Re_{cr}, one given by the hydrodynamic mode (Re^1_{cr} = 493.5) and another given by the new lobe (Re^2_{cr} = 230.49). But here it is noticed that the second lobe doesn't appear and the hydrodynamic mode has similar characteristics as that of the previous case, $K = 1 \times 10^{-6}$ with a slightly lower Re_{cr}. The maximum amplification rate was also close to the previous case. This led to the testing of neutral curves for various values of K from 5×10^{-6} to 2×10^{-2} to check the presence of multiple lobes in the neutral curve. This difference of present results from that in [2] is solely due to the use of wrong dispersion relation in the latter, as opposed to the correct value given by Equation (43). However presence of second lobe of the neutral curve has been noted for the rotating disk problems in [22–24] for compressible boundary layer over a flat plate.

Table 4: Critical parameters and highest growth rates of unstable waves

Case	K	Re_{cr}	ω_{cr}	k^m_{imag}
1	0.0	519.086	0.1391780	-0.0123383
2	1×10^{-6}	518.982	0.1391880	-0.0127017
3	3×10^{-6}	518.776	0.1392180	-0.0127046
3	4×10^{-6}	518.672	0.1392180	-0.0127061
5	5×10^{-6}	518.567	0.1392280	-0.0127076
6	1×10^{-5}	518.045	0.1392770	-0.0127150
7	3×10^{-5}	518.970	0.1394760	-0.0127447
8	3×10^{-4}	489.278	0.1421810	-0.0131611
9	9×10^{-4}	436.947	0.1482090	-0.0141918
10	1×10^{-3}	429.072	0.1492150	-0.0143509
11	2×10^{-3}	360.964	0.1592670	-0.0164150
12	3×10^{-3}	308.281	0.1692450	-0.0187887
13	4×10^{-3}	266.696	0.1791020	-0.0218107
14	5×10^{-3}	233.249	0.1888060	-0.0256166
15	9×10^{-3}	147.901	0.2259400	-0.0464789
16	2×10^{-2}	53.000	0.1707670	-0.0646117

(a) k_{imag} contours

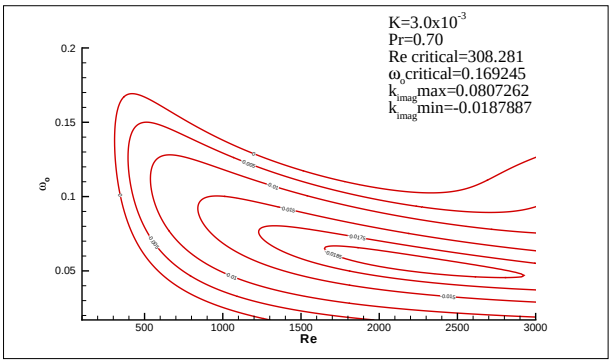

(b) k_{real} contours

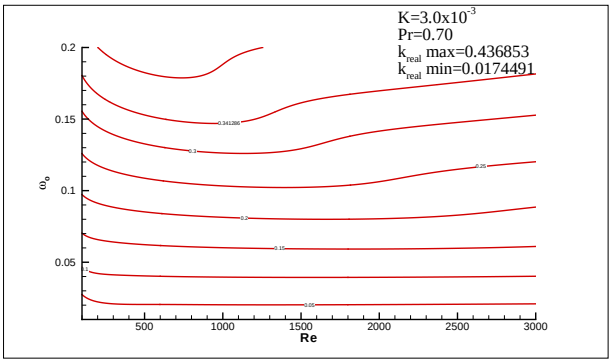

Figure 5: Wave number (k) contours for $K = 3 \times 10^{-3}$. Figure 5(a) shows the imaginary part of k and Figure 5(b) shows the real part of k

In none of the tested cases with other values of K, additional lobes were observed. This indicates that the linear stability analysis do not predict any abrupt changes in the stability properties when heat transfer is present. Results show a steady decrease in Re_{cr} values and an increase in ω_{cr} and maximum growth rate exponent (k_m) values as K is increased. Thus, there is no particular buoyancy parameter beyond which there is a discrete jump in instability properties. All the critical parameters of the neutral curves tested are given in Table 4.

Above $K = 1\times10^{-3}$, the decrease in Re_{cr} for each increment in K by 1×10^{-3} is considerably higher when compared with lower ranges of K. Figure 5(a) shows the neutral curve for $K = 3 \times 10^{-3}$. At $K = 3 \times 10^{-3}$, the upper branch of the neutral curve shows a diverging nature. This implies that there are frequencies which once become unstable, remain so for all higher Re. That is, such instabilities are prevalent in the corresponding inviscid flow also. The lower branch is also found not to exist at higher Re. This region at low ω required quadruple computing. The curve did not reach the $\omega = 0$ line. The Re value at which the upper branch diverges continued to decrease as K is increased. This shows a larger region of instability at higher K as the mean flow is made more and more unstable. For $K = 2 \times 10^{-2}$, the neutral curve does not have the upper branch at all. So increasing the buoyancy parameter makes the boundary layer more and more unstable and prone to early transition over a wider range of frequency from a shorter distance from the leading edge. In Figures 3(b), 4(b) and 5(b), the contours of real part of wave numbers (k_{real}) are shown.

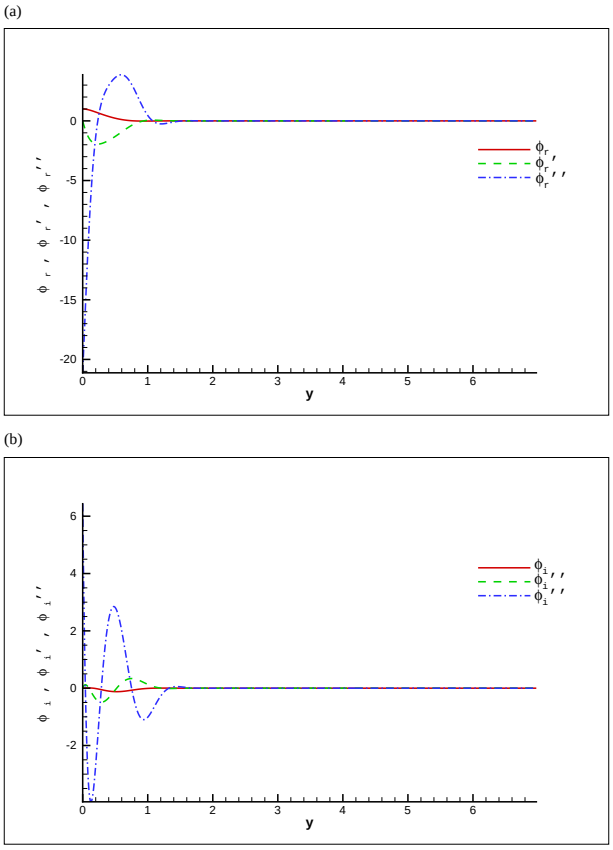

Figure 6: Eigenfunctions obtained for $K = 1 \times 10^{-6}$. Figure 6(a) shows the real part of the disturbance amplitude function, its first and second derivatives and Figure 6(b) shows the corresponding imaginary parts

In Figures 6(a) and 6(b), the real and imaginary parts of the eigenfunctions are plotted for the case $K = 1 \times 10^{-6}$. Equation (49) has been solved for obtaining the eigenfunctions. Equation (49) being an ODE

with known coefficients (obtained through CMM), can be solved using standard Runge-Kutta method. Here the wall conditions for ϕ and ϕ' and freestream conditions for ϕ, ϕ' and ϕ'' are known. The wall condition for ϕ'' is obtained through Newton-Raphson root finding method. At the wall, $\phi_{real} = 1.0$, $\phi_{imag} = 0.0$ and $\phi' = 0$. At the freestream, $\phi = 0$, $\phi' = 0$ and $\phi'' = 0$. It can be seen that ϕ, ϕ' and ϕ'' decay and tends to 0 as we approach the freestream.

6. SUMMARY AND CONCLUSIONS

Spatial stability analysis is carried out and neutral curve obtained for mixed convection boundary layer developing over a heated horizontal plate. The mean flow is obtained by solving the equations (13) and (15) based on the similarity solution provided in [1]. Such boundary layers are characterized by the buoyancy parameter ($K = Gr/Re^{5/2}$) and solved for only adiabatic wall conditions.

Under parallel flow assumptions, the spatial stability problem has been reformulated using the compound matrix method based on earlier work of [2, 14, 17, 19] for hydrodynamic stability problems. CMM allows the stability equations to be solved using standard ODE solving techniques by removing the *stiffness* of the equations at the formulation stage itself. This also allows obtaining the eigenspectrum without any spurious values. This analysis which incorporated modified dispersion relation and initial conditions for the compound variables, showed that there is no multiple nature of the neutral curve for any buoyancy parameter value as was reported in [2]. Some representative eigenspectrum are shown in Tables 1-3. The properties in Table 1 for first three modes are similar to that of Blasius profile obtained by solving a fourth-order system. This provides validation for the methodologies adopted here for the mixed convection problem.

In Figures 3-5, the neutral curve and associated critical parameters and maximum growth rates have been shown for various buoyancy parameters. K values from 1×10^{-6} to 2×10^{-2} were investigated for multiple lobed neutral curves. In none of these cases a thermal mode was found. Thus it has to be understood that, linear stability analysis for mixed convection flow do not predict a buoyancy parameter beyond which the stability characteristics show a sudden qualitative change. The critical Reynolds number (Re_{cr}) kept on decreasing and the critical circular frequency (ω_{cr}) as well as the maximum amplification exponent kept on increasing as K was increased. It can be understood that the effect of increasing the buoyancy parameter is to destabilize the mean flow. Table 4 lists the critical parameters for various cases investigated. The multiple nature of the neutral curves obtained in [2] has to be associated with the incorrect dispersion relation and the corresponding initial conditions for the compound variables. The real and imaginary parts of the disturbance amplitude function for $K = 1 \times 10^{-6}$ are shown Figures 6(a) and 6(b) respectively.

REFERENCES

[1] Schneider, W. (1979). A similarity solution for combined forced and free convection flow over a horizontal plate. *Int. J. Heat Mass Transfer, 22*(10), 1401-1406.

[2] Sengupta, T. K., & Venkata Subbaiah, K. (2006). Spatial stability for mixed convection boundary layer over a heated horizontal plate. *Studies in Applied Mathematics, 117*(3), 265-298.

[3] Brewstar, R. A., & Gebhart, B. (1991). Instability and disturbance amplification in a mixed-convection boundary layer. *J. Fluid Mech, 229*, 115-133.

[4] Mucoglu, A., & Chen, T. S. (1978). Wave instability of mixed convection flow along a vertical flat plate. *Num. Heat Transfer, 1*(2), 267-283.

[5] Iyer, P. A., & Kelly, R. E. (1974). The stability of laminar free convection flow induced by a heated, inclined plate. *Int. J. Heat Mass Transfer, 17*(4), 517-525.

[6] Tumin, A. (2003). The spatial stability of natural convection flow on inclined plates. *ASME J. Fluid Engg., 125*(3), 428-437.

[7] Steinrück, H. (1994). Mixed convection over a cooled horizontal plate: Non-uniqueness and numerical instabilities of the boundary layer equations. *J. Fluid Mech., 278*, 251-265.

[8] Robertson, G. E., Seinfeld, J. H., & Leal, L. G. (1973). Combined forced and free convection flow pasta horizontal flat plate. *AIChE Jour., 19*(5), 998-1008.

[9] Wang, X. A. (1982). An experimental study of mixed, forced, and free convection heat transfer from a horizontal flat plate to air. *ASME J. Heat Transfer, 104*(1), 139-144.

[10] Gilpin, R. R., Imura, H., & Cheng, K. C. (1978). Experiments on the onset of longitudinal vortices in horizontal Blasius flow heated from below. *ASME J. Heat Transfer, 100*(1), 71-77.

[11] Chen, T. S., & Mucoglu, A. (1979). Wave instability of mixed convection flow along a horizontal flat plate. *Int. J. Heat Mass Transfer, 22*(2), 185-196.

[12] Drazin, P. G., & Reid, W. H. (1981). *Hydrodynamic stability*. Cambridge: Cambridge University Press.

[13] Schmid, P. J., & Henningson, D. S. (2001). *Stability and transition in shear flows*. New York: Springer Verlag.

[14] Allen, L., & Bridges, T. J. (2003). Hydrodynamic stability of the Ekman boundary layer including interaction with a compliant surface: A numerical framework. *European J. Mechanics B/Fluids, 22*(3), 239-258.

[15] Moresco, P., & Healey, J. J. (2000). Spatio-temporal instability in mixed convection boundary layers. *J. Fluid Mech., 402*, 89-107.

[16] Allen, L., & Bridges, T. J. (2002). Numerical exterior algebra and the compound matrix method. *Numerische Mathematik, 92*(2), 197-232.

[17] Ng, B. S., & Reid, W. H. (1985). The compound matrix method for ordinary differential systems. *J. Comp. Phy., 58*(2), 209-228.

[18] Sengupta, T. K., Ballav, M., & Nijhawan, S. (1994). Generation of Tollmien-Schlichting waves by harmonic excitation. *Phys. Fluids, 6*(3), 1213-1222.

[19] Sengupta, T. K. (1992). Solution of Orr-Sommerfeld equation for high wave numbers. *Computers Fluids, 21*(2), 301-303.

[20] Brillouin, L. (1960). *Wave propagation and group velocity*. New York: Academic Press.

[21] Van der Pol, B., & Bremmer, H. (1959). *Operational calculus based on two-sided Laplace integral*. Cambridge: Cambridge University Press.

[22] Turkyilmazoglu, M., Cole, J. W., & Gajjar, J. S. B. (2000). Absolute and convective instabilities in the compressible boundary layer on a rotating disk. *Theoretical and Computational Fluid Dynamics, 14*(1), 21-37.

[23] Turkyilmazoglu, M. (2005). Lower branch modes of the compressible boundary layer flow due to a rotating-disk. *Studies in Applied Mathematics, 114*(1), 17-43.

[24] Mack, L. M. (1969). Boundary layer stability theory. *Doc. 900-277, Rev.* A Jet Prop. Lab, Pasadena, California, JPL.

APPENDIX: COMPOUND MATRIX METHOD FOR MIXED CONVECTION PROBLEM

The general methods for fourth- and sixth-order systems are as given in [17] and the specific formulation given here is applicable to the coupled system of equations (25) and (26). In [2] the mixed convection problem was studied using similar formulation technique, but the choice of the compound variables and associated dispersion relation was incorrect. Here the corrected method is shown. General methodology can be found in [14, 16, 17].

Equations (25) and (26) can be converted to a sixth order ODE in h. An induced system is constructed, determined by the set of asymptotic boundary conditions at $y = Y_\infty$ that in turn is governed by the analytic nature of solution at $y \to \infty$. The system constituted by (25) and (26) was originally a boundary value problem. Through the introduction of the new variables, this is converted to an initial value problem. The main advantage of this procedure is that, it removes the stiffness of the original system. For the sixth-order-system, this method is equivalent to projecting the solution on a subspace of C^6 with the help of three decaying boundary conditions for $y \to \infty$, following the notations of [14], into $\Lambda^3(C^6)$. Similarly, the boundary conditions at $y = 0$ defines a second three-dimensional subspace of C^6. The problem is thus reduced to linking these two three-dimensional subspaces of C^6 satisfying equation (39). Any subspace spanned by three linearly independent vectors $v_1,\ v_2,\ v_3$, is represented notationally as a point $v_1 \Lambda v_2 \Lambda v_3$, in the vector space $\Lambda^3(C^6)$, where Λ is the wedge product[14].

The new basis variables formed are, $e_1 = [\phi_1,\ \phi_3,\ \phi_5]$; $e_2 = [\phi_1',\ \phi_3',\ \phi_5']$; $e_3 = [\phi_1'',\ \phi_3'',\ \phi_5'']$; $e_4 = [\phi_1''',\ \phi_3''',\ \phi_5''']$; $e_5 = [h_1,\ h_3,\ h_5]$; $e_6 = [h_1',\ h_3',\ h_5']$ in C^6, then all the elements of $e_i \Lambda e_j \Lambda e_k$ form the basis for $\Lambda^3(C^6)$ with the dimension ${}^nC_r = 20$. The solution matrix is obtained as

$$\begin{bmatrix} \phi_1 & \phi_3 & \phi_5 \\ \phi_1' & \phi_3' & \phi_5' \\ \phi_1'' & \phi_3'' & \phi_5'' \\ \phi_1''' & \phi_3''' & \phi_5''' \\ h_1 & h_3 & h_5 \\ h_1' & h_3' & h_5' \end{bmatrix}. \tag{A.1}$$

This is different from that was given in [2]. This also changes the dispersion relation given here in Equation (43) as compared to given in Equation (32) of [2]. It has twenty (3×3) minors–that are also called the second compound[17] denoted by

$$y_{ijk} = [e_i e_j e_k]^T, \tag{A.2}$$

where $i = 1, 2, 3, 4$; $j = i + 1, ..., 5$; and $k = j + 1, ...6$. If we let $\mathbf{y} = [y_{123},\ y_{123},\ y_{123},\ ...,\ y_{123}]^T$, then by direct calculation it can be shown that y satisfy the following set of linear coupled first-order equation given by

$$\mathbf{y}' = B(y)\mathbf{y}, \tag{A.3}$$

where the B matrix elements are given in [17] and [14] for sixth-order systems. By listing down the compound matrix variables in a lexicographic fashion, ie., $y_1 \equiv y_{123}$; $y_2 \equiv y_{124}$ ... $y_{20} \equiv y_{456}$, one can obtain the induced system of equations given by Equation (A.3) in [2]. Introduction of the second compounds as the new unknowns of the problem remove its stiffness thus making it possible to use any standard integration procedure to solve it. We know the free stream solution ($y \to \infty$) which makes it possible to specify the initial conditions for the twenty compound variables at the freestream. Hence a boundary value problem is converted into an initial value problem.

Initial Conditions for the Induced System

The wall excitation problem has fundamental solutions decaying exponentially with height. This allows us to truncate domain of investigation up to Y_∞. This is used to convert the initial BVP into an IVP in compound variables. Using the definition of (39) into the definition of second compounds, as given by (A.1), and scaling the resulting expressions by $e^{(k+Q+S)Y_\infty}$ for positive real parts of k, Q and S, one gets

$$y_{1\infty} = [S^2(k-Q) + Q^2(S-k) + k^2(Q-S)]\gamma,$$

$$y_{2\infty} = [-S^3(k-Q) - Q^3(S-k) - k^3(Q-S)]\gamma,$$

$$y_{3\infty} = (k-Q), y_{4\infty} = S(Q-k),$$

$$y_{5\infty} = [S^3(k^2-Q^2) + Q^3(S^2-k^2) + k^3(Q^2-S^2)]\gamma,$$

$$y_{6\infty} = (Q^2-k^2), y_{7\infty} = S(k^2-Q^2),$$

$$y_{8\infty} = (k^3-Q^3), y_{9\infty} = S(Q^3-k^3),$$

$$y_{10\infty} = 0, y_{11\infty} = [S^3(kQ^2-k^2Q) + Q^3(Sk^2-S^2k) + k^3(QS^2-Q^2S)]\gamma,$$

$$y_{12\infty} = Qk(k-Q), y_{13\infty} = QSk(Q-k),$$

$$y_{14\infty} = Qk(Q^2-k^2), y_{15\infty} = -QSk(Q^2-k^2),$$

$$y_{16\infty} = 0, y_{17\infty} = Q^2k^2(k-Q),$$

$$y_{18\infty} = Q^2Sk^2(Q-k), y_{19\infty} = 0 \;\&\; y_{20\infty} = 0.$$

For evaluating Q and S cases with positive real part are taken. But this restriction is not there if the response field is obtained by integrating (A.2) along the Bromwich contour. While the individual components of the solution ϕ (Equation (37)) decays at widely different rates due to the disparate value of characteristic exponents, the second compounds $\mathbf{y}$, all have the same decay rate given by the exponent $(k+Q+S)Y_\infty$. This is how CMM removes the stiffness problem associated with with the original differential equations. Now the induced system of equations can be integrated as an IVP from $y = Y_\infty$ to wall ($y = 0$) by any standard ODE solving technique. For solving this particular problem, four-stage Runge-Kutta method has been used.